Journal of Molecular and Cellular Cardiology 66 (2014) 126–132

Contents lists available at ScienceDirect

Journal of Molecular and Cellular Cardiology

journal homepage: www.elsevier.com/locate/yjmcc

Original article

Inhibition of endocannabinoid-degrading enzyme fatty acid amide hydrolase increases atherosclerotic plaque vulnerability in mice

Friedrich Felix Hoyer [a,*,1], Mona Khoury [a,1], Heike Slomka [a], Moritz Kebschull [e], Raissa Lerner [b], Beat Lutz [b], Hans Schott [c], Dieter Lütjohann [c], Alexandra Wojtalla [d], Astrid Becker [d], Andreas Zimmer [d], Georg Nickenig [a]

[a] Klinik II für Innere Medizin, Universität Bonn, 53125 Bonn, Germany
[b] Institut für physiologische Chemie, Johannes Gutenberg Universität Mainz, 55128 Mainz, Germany
[c] Institut für klinische Chemie und klinische Pharmakologie, Universität Bonn, 53125 Bonn, Germany
[d] Institut für molekulare Psychiatrie, Universität Bonn, 53125 Bonn, Germany
[e] Zentrum für Zahn-, Mund-, und Kieferheilkunde, Universität Bonn, 53125 Bonn, Germany

ARTICLE INFO

Article history:
Received 25 June 2013
Received in revised form 14 November 2013
Accepted 18 November 2013
Available online 25 November 2013

Keywords:
Fatty acid amide hydrolase
Atherosclerosis
URB597
Vascular inflammation

ABSTRACT

The role of endocannabinoids such as anandamide during atherogenesis remains largely unknown. Fatty acid amide hydrolase (FAAH) represents the key enzyme in anandamide degradation, and its inhibition is associated with subsequent higher levels of anandamide. Here, we tested whether selective inhibition of FAAH influences the progression of atherosclerosis in mice. Selective inhibition of FAAH using URB597 resulted in significantly increased plasma levels of anandamide compared to control, as assessed by mass spectrometry experiments in mice. Apolipoprotein E-deficient ($ApoE^{-/-}$) mice were fed a high-fat, cholesterol-rich diet to induce atherosclerotic conditions. Simultaneously, mice received either the pharmacological FAAH inhibitor URB597 1 mg/kg body weight ($n = 28$) or vehicle ($n = 25$) via intraperitoneal injection three times a week. After eight weeks, mice were sacrificed, and experiments were performed. Vascular superoxide generation did not differ between both groups, as measured by L012 assay. To determine whether selective inhibition of FAAH affects atherosclerotic plaque inflammation, immunohistochemical staining of the aortic root was performed. Atherosclerotic plaque formation, vascular macrophage accumulation, as well as vascular T cell infiltration did not differ between both groups. Interestingly, neutrophil cell accumulation was significantly increased in mice receiving URB597 compared to control. Vascular collagen structures in atherosclerotic plaques were significantly diminished in mice treated with URB597 compared to control, as assessed by picro-sirius-red staining. This was accompanied by an increased aortic expression of matrix metalloproteinase-9, as determined by quantitative RT-PCR and western blot analysis. Inhibition of fatty acid amide hydrolase does not influence plaque size but increases plaque vulnerability in mice.

1. Introduction

Atherosclerosis is a chronic inflammatory disease and remains the main cause of death in the industrialized world [1]. During atherogenesis, stable atherosclerotic lesions are generally rich in smooth muscle cells and extracellular matrix and can remain asymptomatic for years. Extensive accumulation of inflammatory cells, particularly monocyte-derived macrophages, delivers matrix digesting enzymes that render the lesion unstable [2]. Advanced, unstable atherosclerotic plaques are characterized by a thin fibrous cap that is weak and prone to rupture [2]. If the cap ruptures, exposure of thrombogenic tissues causes a sudden thrombotic occlusion of the vessel with potentially lethal consequences, such as myocardial infarction [3]. Mechanisms that govern plaque-stability are clinically of utmost importance, since they control progression of stable to unstable disease conditions [2].

Recent work has demonstrated a crucial influence of the endocannabinoid system on vascular inflammation and atherosclerosis in mice [4,5]. The endocannabinoid system primarily consists of two G-protein coupled receptors. While the cannabinoid receptor 1 (CB1) is mainly responsible for various psychotropic effects, the peripheral cannabinoid receptor 2 (CB2) particularly mediates anti-inflammatory effects in several disease models [5–9]. Both receptors are endogenously activated by two endocannabinoids called anandamide (AEA) and 2-arachidonoylglycerol (2-AG). 2-AG activates CB1 and CB2, while AEA more intensively stimulates CB1, but also activates CB2 [10]. AEA is degraded by the enzyme fatty acid amide hydrolase (FAAH), which can be selectively blocked by several compounds such as URB597 [11]. Genetic deletion as well as pharmacological inhibition of FAAH are followed by significantly increased levels of AEA in various tissues [11–17]. In the context of atherosclerosis, administration of exogenous cannabinoid receptor agonists, such as Δ^9-tetrahydrocannabinol

* Corresponding author at: Medizinische Klinik und Poliklinik II, Universitätsklinikum Bonn, 53105 Bonn, Germany. Tel.: +49 228 287 51487; fax: +49 228 287 51482.
E-mail address: felix.hoyer@ukb.uni-bonn.de (F.F. Hoyer).
[1] Both authors contributed equally.

0022-2828/$ – see front matter © 2013 Elsevier Ltd. All rights reserved.
http://dx.doi.org/10.1016/j.yjmcc.2013.11.013

(THC), WIN 55.212 and JWH 133, can beneficially regulate the extent of vascular inflammation and eventually attenuate lesion formation via the activation of CB2 in mice [5,18–20]. With regards to plaque vulnerability, activation of CB2 increases plaque stability by down-regulation of plaque-destabilizing enzymes [21], while unstable human carotid plaques are characterized by diminished expression of CB2. The role of CB1 for atherosclerotic plaque vulnerability remains largely unknown though it has been shown that inhibition of CB1 is associated with atheroprotective properties. It has been suggested that pharmacological inhibition of CB1 reduces atherosclerotic plaque burden in mice [22]. Work of our own group did not detect any influence on plaque size, however, inhibition of CB1 resulted in impaired vascular oxidative stress and improved endothelial function [23]. Both studies suggest that CB1 inhibition mediates atheroprotective effects. Differences regarding atherosclerotic lesion size may be based on different experimental settings since different mouse models were used for both studies. Here, we sought to examine whether endogenous CB1 activation via inhibition of FAAH influences atherogenesis and plaque inflammation in a mouse model of atherosclerosis.

2. Materials and methods

2.1. Material

The selective FAAH inhibitor URB597 was purchased from Enzo Life Science. L012 was obtained from Wako Chemicals. Oil red O, salts and other substances were purchased from Sigma.

2.2. Mass spectrometry and treatment of animals

In order to determine whether intraperitoneal application of URB597 affects the levels of endocannabinoids, wild-type mice (each group $n = 5$) were subjected either to 1 mg/kg body weight URB597 via intraperitoneal injection or to an equivalent amount of vehicle for three days per week. Then, mice were sacrificed, blood was drawn and mass spectrometry experiments were performed, as recently described [20].

Apolipoprotein E-deficient mice ($ApoE^{-/-}$) (C57BL/6 genetic background, Charles River) were kept in a 22 °C room with a 12 hour light/dark cycle and received water ad libitum. At the age of 10 weeks, mice were fed a high-fat, cholesterol-rich diet that contained 21% fat, 19.5% casein and 1.25% cholesterol (Ssniff). Simultaneously, mice received URB597 1 mg/kg body weight ($n = 28$) or vehicle (5% DMSO) ($n = 25$) via intraperitoneal injection three times per week. The chosen dosage is in accordance with other studies investigating pharmacological effects of URB597 in animal models [24–26]. Systolic blood pressure and heart rate were assessed by a computerized tail cuff system (BP-2000, Visitech System) in conscious animals. Mice were accustomed to the prewarmed tail cuff device for three days. Then, systolic blood pressure and heart rate were monitored for three days. After eight weeks of treatment, mice were sacrificed, blood was drawn, and organs were instantly procured. Plasma cholesterol levels were analyzed using gas chromatography–flame ionization detection, as recently described [20]. All experiments were done in accordance with the German animal protection law.

2.3. Measurement of reactive oxygen species

Reactive oxygen species (ROS) were determined using the L012 chemiluminescence method. L012 is derived from luminol that has a high sensitivity for detecting superoxide radicals. Luminol does not show redox cycling itself. Mouse aortas were carefully cut into small segments and were placed in modified Krebs-Hepes buffer. Adipose tissue was removed. After that, 2-mm aortic segments were put into scintillation vials containing Krebs-Hepes buffer with 100 μmol/l L012 and were incubated for 5 min. Chemiluminescence was detected for 10 min in a scintillation counter (Lumat 9501, Berthold) in 1-minute intervals. The 5-minute value was used for analysis. After assessment of chemiluminescence, aortic segments were dried and weighed. Vascular superoxide release is expressed as relative luminescent units (RLU) per milligram of aortic tissue and minute.

2.4. Assessment of atherosclerotic plaque formation

Murine hearts were excised and immediately embedded in tissue TEC (OCT embedding mediums, Miles), snap-frozen and stored at −80 °C. After that, sections through the aortic sinus were obtained using a Leica cryostat (9 μm). Oil red O staining was performed to detect atherosclerotic plaque formation. Samples were fixed with 3.7% formaldehyde for 1 h, rinsed with deionized water and placed in Oil red O working solution (0.5%) for 15 min. Sections were rinsed again and stained with hematoxylin. To quantify the extent of vascular atherosclerosis, sections were analyzed under a microscope (Zeiss). Axio vision software was used for macroscopic analysis. Plaque formation was determined as total plaque size in mm^2 per aortic sinus.

2.5. Assessment of vascular monocyte and macrophage accumulation

Sections were generated as described above using a Leica cryostat. To analyze the accumulation of monocytes and macrophages in the vessel wall, Moma-2 (Acris, SM065) staining was performed. Sections were fixed in acetone for 45 min, and then blocked with normal goat serum for 30 min. Sections were incubated with Moma-2 for 1 h and subsequently rinsed with 0.1 mol Tris (pH 6.8). Afterwards, the second antibody was added for 1 h. Fast-red color complex was employed to detect Moma-2 positive areas. Sections were stained with hematoxylin for 1 min and, finally, washed with lukewarm water for 15 min. Axio vision software was used for macroscopic analysis. Cell accumulation is expressed as Moma-2 positive area per total area of vessel wall in %.

2.6. Assessment of collagen structures in atherosclerotic plaques

To analyze the collagen content in atherosclerotic plaques, picrosirius-red staining was carried out in accordance to standard protocols. The picro-sirius-red solution was prepared one week before staining by desolving 0.1 g Direct Red 80 (Sigma-Aldrich, Germany) in 100 ml 1.2% picric acid. Sections were finally covered with entellan and cover glasses. To quantify the extent of collagen in vascular atherosclerosis, sections were examined under a microscope (Zeiss) with polarization filter. In bright-field microscopy collagen appears as a red area on lutescent ground. In polarization microscopy, collagen fibers are orange up to red. Collagen structures were quantified using Axio vision software and the total amount of collagen structures was divided by the plaque size, leading to a ratio collagen content per atherosclerotic lesion.

2.7. Assessment of neutrophil accumulation in atherosclerotic plaques

Sections were fixed in acetone for 30 min. The endogenous peroxidase was blocked with 1% H_2O_2 in methanol. Then, sections were blocked with normal goat serum for 30 min, and incubated with the primary antibody (Ly6G, BD 551459). After incubation with the second antibody, fast-red color complex was used to stain Ly6G positive areas in atherosclerotic lesions, and sections were counterstained with hematoxylin. Axio vision software was used for analysis. Neutrophil accumulation is shown as Ly6G positive area per plaque.

2.8. Analysis of circulating inflammatory cells

Mouse blood samples were analyzed as previously described [20]. Following red cell lysis, the viable lymphocyte population was analyzed for CD14 (Becton Dickinson 553739, NJ, USA) and for CD3 (Becton

Dickinson 555275, NJ, USA). Isotype identical antibodies and unstained samples were used as controls. Cell fluorescence was determined immediately after staining with a FACSCalibur instrument (Becton Dickinson, NJ, USA). Data was analyzed using Cell Quest software (Becton Dickinson, NJ, USA). Units of all measured components are specific events obtained after measuring 20,000 events in a pre-specified lymphocyte gate during FACS analysis.

2.9. Real-time PCR

Real-time RT-PCR was carried out in order to determine gene expression of matrix metalloproteinases −2 and 9. Aortas of ApoE$^{-/-}$ mice treated with either URB597 or vehicle were carefully excised and homogenized using a motorized homogenizer (Precellys, Bertin Technologies, Montigny-le-Bretonneux, France). Then, RNA was isolated with peqGOLD RNA-Pure (peqLAB Biotechnology, Erlangen, Germany). RNA concentration and quality were assessed with a spectrometer. Next, 1 μg of RNA was reversed transcribed with an Omniscript RT Kit (Qiagen, Hilden, Germany). The single-stranded cDNA was amplified by real-time quantitative reverse transcription-polymerase chain reaction (RT-PCR) with a TagMan system (ABI-7500 fast PCR System, Carlsbad, California, USA). Primer for MMP-2: forward 5′-GTC GCC CCT AAA ACA GAC AA -3′ and reverse: 5′-GGT CTC GAT GGT GTT CTG GT-3′, and for MMP-9 forward: 5′-AAC ACC ACC GAG CTA TCC AC-3′ and reverse: 5′-AGG AGT CTG GGG TCT GGT TT-3′. For quantification, mRNA levels were normalized to endogenous 18s rRNA. In both cases, quantitative RT-PCR was performed in triplicates in a total volume of 20 μl containing SYBR Master Green 9 Mix (Applied Biosystems, CA, USA), DNAse/RNAse free water (Invitrogen), 1 μl of cDNA and 0.2 μl of each primer. Reaction was measured using 7500 Fast Real-Time PCR-System and 7500 Fast System SDS Software (Applied Biosystems).

2.10. Western blot and zymography

Western blot experiments were carried out in accordance to standard protocols. Briefly, whole aortic tissue lysates were used for experiments and protein content was measured using the Lowry method. 100 μg of protein was resolved by SDS-PAGE and electrophoretically transferred on nitrocellulose membranes (VWR) which were blocked by 2.5% BSA in PBS. The primary antibody (MMP-9) was purchased from R&D (AF909) and used at a dilution of 1:250. The second antibody was HRP anti-goat IgG (Sigma 115 K4809) and used at a dilution of 1:2000. GAPDH (Hytest Ltd. 5G4Mab6C5) was used as endogenous control. To account for possible differences in protein load, measurements were presented as a ratio of the MMP-9 signal to the respective GAPDH signal. Zymography experiments were performed in accordance to standard protocols. Plasma activity of MMP-9 was assessed by gelatin zymography. In brief, protein content of plasma samples was measured using the lowry method, and equal amounts of protein (50 μg) were subjected to a 0.1%-gelatin gel electrophoresis in Tris-Glycine SDS Running Buffer (Carl Roth). Sample buffer served as negative control. Gels were renaturated in 2.5% Triton X-100 for 30 min, then placed in development buffer (Bio-Rad) for 30 min at room temperature. Thereafter, gels were incubated in fresh buffer for 48 h at 37 °C. Staining was performed using a 0.5% Coomassie solution (40% Methanol, 10% Acetic acid, 50% Aqua dest.). Proteolysis of the active MMP-9 form was detected as white bands against dark background at 88 kDa. The

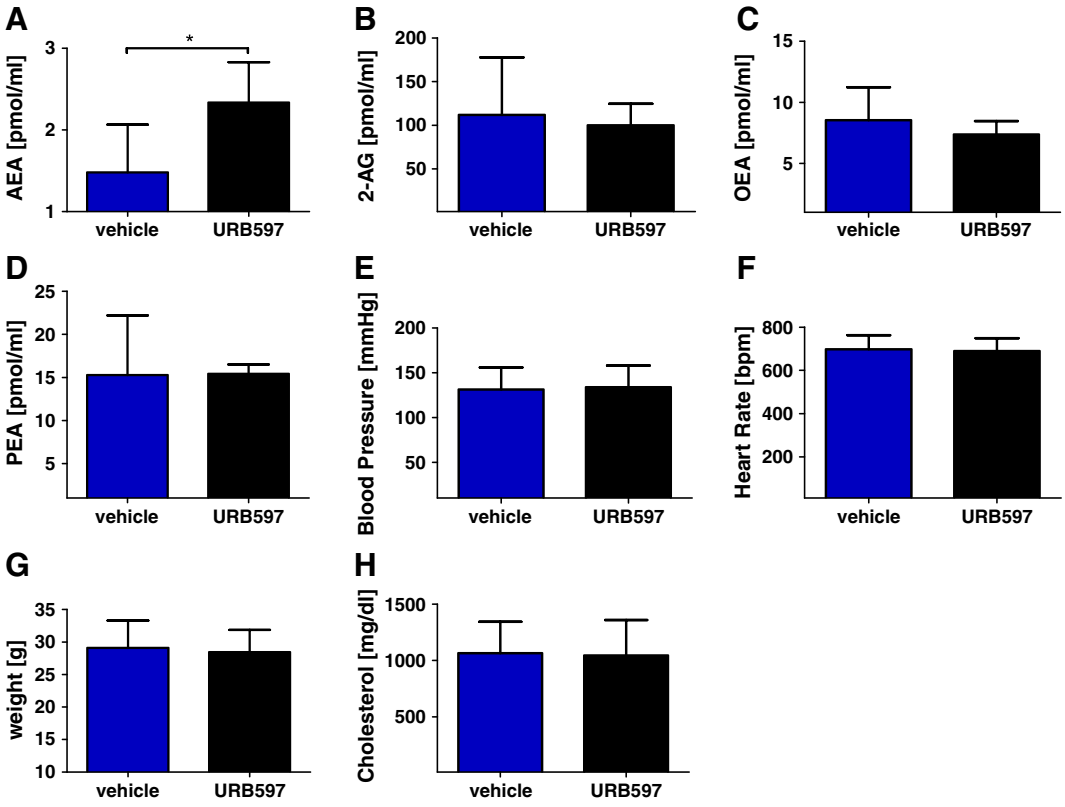

Fig. 1. Plasma levels of endocannabinoids were determined via mass spectrometry in wild-type mice receiving either URB597 (1 mg/kg body weight) or an equivalent amount of vehicle. (A) Treatment with URB597 significantly increased plasma levels of AEA compared to control (2.34 ± 0.5 vs. 1.48 ± 0.58 pmol/ml, $p < 0.05$). The levels of other endocannabinoids and related compounds did not differ between both groups: (B) 2-Arachidonoylglycerol (2-AG; 99.85 ± 24.62 vs. 111.7 ± 65.85 pmol/ml, $p > 0.05$), (C) Oleoylethanolamine (OEA; 7.38 ± 1.1 vs. 8.54 ± 2.69 pmol/ml, $p > 0.05$) and (D) Palmitoyl ethanolamide (PEA; 15.42 ± 1.1 vs. 15.28 ± 6.92 pmol/ml, $p > 0.05$). (E) Blood pressure, (F) heart rate, (G) weight and (H) cholesterol levels were determined in ApoE$^{-/-}$ fed a high-fat, cholesterol-rich diet for eight weeks treated either with URB597 (1 mg/kg body weight) or vehicle. No differences were observed between the groups.

integrated optical density (IOD) of bands was quantified using LabWorks software.

2.11. Statistical analysis

Statistical analysis was performed using R 3.0.2 and GraphPad Prism V (GraphPad Inc., San Diego, CA, USA). Data are shown as mean ± SD. Normal distribution was assessed by the Kolmogorov–Smirnov with Dallal-Wilkinson-Lilliefor P value and D'Agostino & Pearson omnibus normality testing. Statistical analysis was performed using unpaired Student's t-tests. Effect sizes (Cohen's d) were calculated using the compute.es package. $p < 0.05$ denotes statistical significance.

3. Results

3.1. Inhibition of FAAH increases plasma levels of AEA

In order to determine whether application of 1 mg/kg body weight URB597 influences the levels of endocannabinoids in mice, mass spectrometry experiments were performed. Mice treated with URB597 ($n = 5$) had significantly increased plasma levels of AEA as compared with vehicle-treated mice ($n = 5$) (2.34 ± 0.5 vs. 1.48 ± 0.58 pmol/ml, $p < 0.05$). The plasma level of other endocannabinoids and related compounds, such as 2-AG, Palmitoyl ethanolamide (PEA) and Oleoyl ethanolamine (OEA) did not differ between both groups (Fig. 1). Cholesterol levels, blood pressure and heart rate were assessed after eight weeks of a high-fat, cholesterol-rich diet. There were no differences between the groups.

3.2. Inhibition of FAAH and plaque inflammation

Atherosclerotic plaque extent was assessed in the aortic sinus after eight weeks of a high-fat, cholesterol-rich diet by means of Oil red O staining. Treatment with URB597 did not influence atherosclerotic plaque burden compared with control (0.41 ± 0.15 vs. 0.42 ± 0.11 mm^2, $p = 0.83$, Cohen's $d = 0.06$), (Fig. 2A). In order to assess vascular accumulation of macrophages, Moma-2 staining was carried out. No differences were observed between both groups (0.39 ± 0.16 vs. 0.41 ± 0.14 in %, $p = 0.78$, Cohen's $d = 0.11$), (Fig. 2B). T cell accumulation, as assessed by anti-CD3 staining, revealed no differences between both groups as well (126.5 ± 109.5 vs. 140.9 ± 109.4, $p = 0.65$, Cohen's $d = 0.13$; Fig. 2C). Accumulation of neutrophils

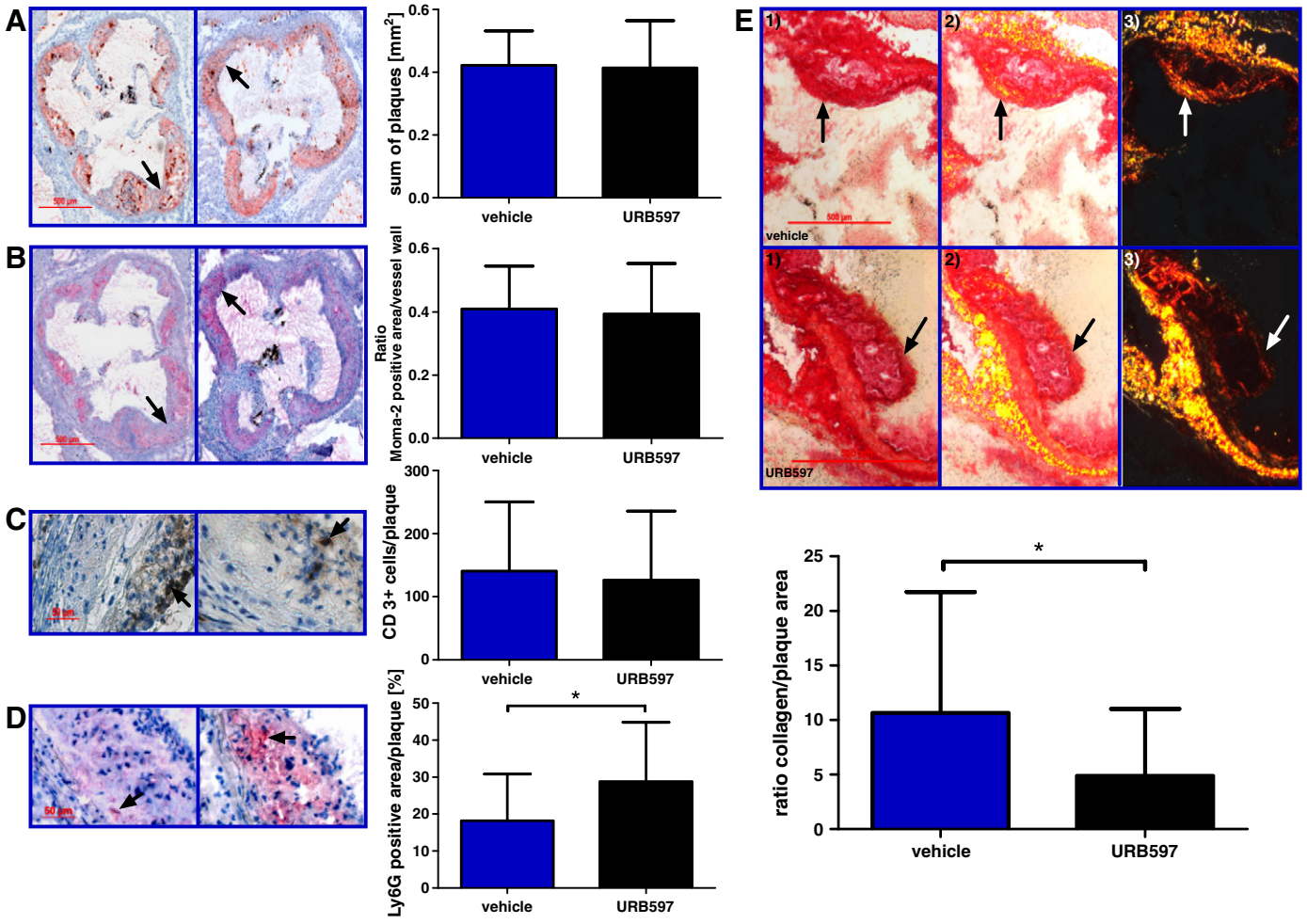

Fig. 2. Atherosclerotic lesion formation and accumulation of inflammatory cells. After 8 weeks of a high-fat, cholesterol-rich diet atherosclerotic lesion size was assessed in the aortic sinus by means of Oil red O staining. (A) Lesion size did not differ in $ApoE^{-/-}$ mice treated with URB597 compared to $ApoE^{-/-}$ mice treated with vehicle (0.41 ± 0.15 vs. 0.42 ± 0.11 mm^2, $p > 0.05$). (B) Monocyte/macrophage accumulation did not differ between both groups as well (0.39 ± 0.16 vs. 0.41 ± 0.14, $p > 0.05$). (C) T cell accumulation was assessed using anti-CD3-staining. There were no significant differences between the groups (126.5 ± 109.5 vs. 140.9 ± 109.4, $p > 0.05$). (D) Neutrophils in atherosclerotic lesions were detected by staining of Ly6G. In mice treated with URB597, the numbers of neutrophils in atherosclerotic lesions were significantly increased compared to control (28.82 ± 16 vs. 18.19 ± 12.62, $p < 0.05$). (E) Collagen structures in the atherosclerotic plaque were determined by means of picro-sirius-red staining. Treatment with URB597 significantly diminished the amount of collagen structures compared to vehicle (4.88 ± 6.16 vs. 10.66 ± 11.07, $p < 0.05$). The collagenous cap (white arrow) that covers atherosclerotic lesions was significantly diminished in mice that were treated with URB597 compared to vehicle-treated mice. Atherosclerotic lesions were examined with 1) bright-field microscopy, 2) bright-field microscopy combined with polarization microscopy and 3) polarization microscopy.

was assessed using anti-LY6G staining. Mice treated with URB597 exhibited significantly increased levels of neutrophils compared to control (28.82 ± 16 vs. 18.19 ± 12.62 in %, $p < 0.05$; Fig. 2E).

3.3. Circulating inflammatory cells

Circulating cells such as monocytes/macrophages and T cells contribute to atherogenesis by invading the vascular wall and propagating inflammatory processes. In order to assess possible effects of FAAH inhibition on the numbers of circulating cells, flow cytometry experiments were performed. The levels of circulating CD14 positive macrophages did not differ between both groups (0.44 ± 0.57 vs. 0.45 ± 0.57 in %, $p > 0.05$; Fig. 3E). The levels of CD3 positive T cells did not differ as well (27.4 ± 9.7 vs. 31.3 ± 10.3 in %, $p > 0.05$; Fig. 3D).

3.4. Inhibition of FAAH does not modulate vascular reactive oxygen species generation

Reactive oxygen species (ROS) were measured by L012 chemiluminescence assays in intact aortic segments of ApoE$^{-/-}$ mice treated either with URB597 or vehicle. Treatment with the selective FAAH inhibitor did not significantly affect the liberation of reactive oxygen species compared to control (Fig. 3A).

3.5. Inhibition of FAAH reduces collagen structures in atherosclerotic lesions

In order to assess collagen structures in atherosclerotic plaques, picro-sirius-red staining was carried out as described above (Fig. 2D). Vascular collagen content was significantly diminished in mice treated with URB597 compared to mice treated with vehicle (4.88 ± 6.16 vs. 10.66 ± 11.7 in %, $p < 0.05$, Cohen's $d = 0.67$).

3.6. Inhibition of FAAH increases aortic expression and plasma activity of matrix-degrading enzyme MMP-9

In order to gain more insights into the underlying vascular processes, abdominal aortic tissue of both groups was obtained, and quantitative RT-PCR experiments were performed. Treatment with URB597 did not significantly affect the expression of matrix metalloproteinase-2 (1.59 ± 1.55 vs.1 ± 0.63, $p > 0.05$; Fig. 3B), however, the expression of matrix metalloproteinase-9 was significantly increased compared to control (4.16 ± 6.39 vs. 1 ± 0.88, $p < 0.05$; Fig. 3C). Increased expression of MMP-9 in aortic tissue of mice treated with URB597 was confirmed by western blot experiments (Fig. 3D). Plasma activity of MMP-9 was assessed by zymography experiments. Treatment with URB597 significantly increased plasma activity of MMP-9 compared to control (Fig. 3G).

4. Discussion

This study investigates the role of fatty acid amide hydrolase during atherogenesis in mice. Inhibition of FAAH significantly increased the plasma levels of AEA with consecutively enhanced cannabinoid receptor activation. Inhibition of FAAH in ApoE$^{-/-}$ mice, which were fed a high-fat, cholesterol-rich diet for eight weeks, did influence neither the extent of atherosclerotic plaque burden nor the accumulation of

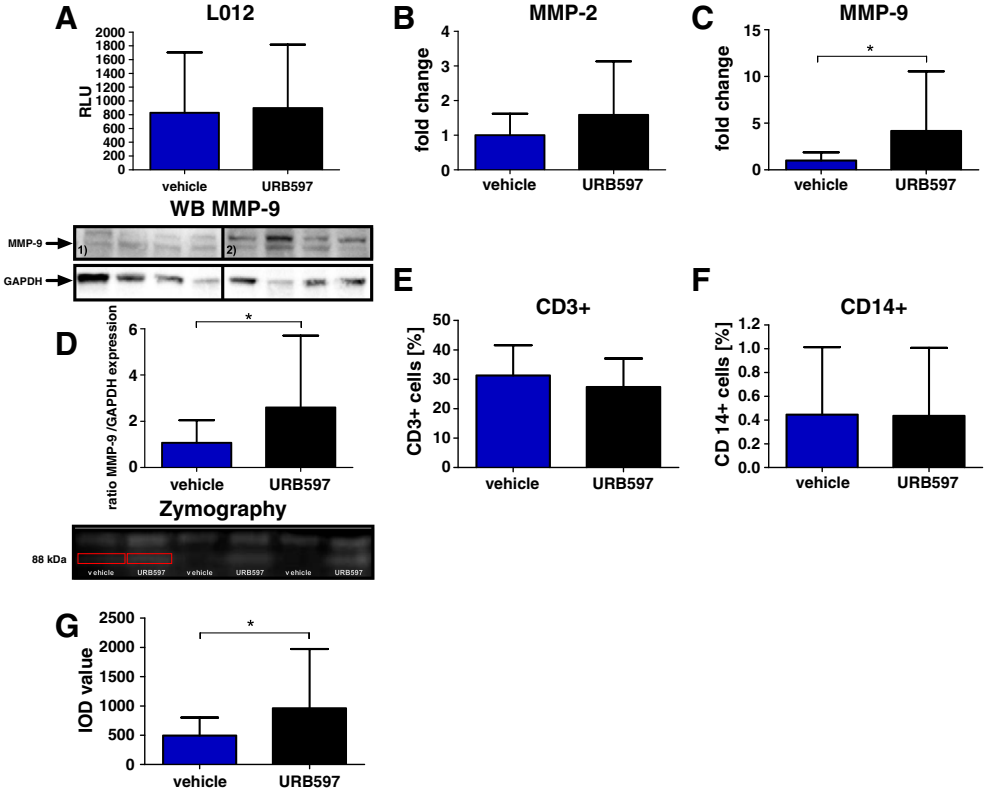

Fig. 3. Reactive oxygen species, matrix metalloproteinases and circulating inflammatory cells. (A) Aortic release of reactive oxygen species was determined by L012 chemiluminescence. There were no differences between ApoE$^{-/-}$ mice treated with URB597 compared to vehicle treated ApoE$^{-/-}$ mice (897.4 ± 922.4 vs. 828.7 ± 875.6 RLU, $p > 0.05$). Aortic expression of matrix metalloproteinases was assessed by quantitative RT-PCR. While treatment with URB597 did not significantly influence the expression of MMP-2 (1.59 ± 1.55 vs. 1 ± 0.63, $p > 0.05$) (B), the expression of MMP-9 was significantly increased in ApoE$^{-/-}$ mice treated with URB597 compared to ApoE$^{-/-}$ mice treated with vehicle (4.16 ± 6.39 vs. 1 ± 0.88, $p < 0.05$) (C). (D) Increased aortic expression of MMP-9 was confirmed by western blot analysis (2.60 ± 3.11 vs. 1.07 ± 0.98, $p < 0.05$); 1) vehicle 2) URB597 treated. Circulating inflammatory cells were assessed via flow cytometry. Treatment with URB597 did not affect the levels of (E) CD3 positive T cells (27.4 ± 9.7 vs. 31.3 ± 10.3%, $p > 0.05$) and (F) CD14 positive macrophages (0.44 ± 0.57 vs. 0.45 ± 0.57%, $p > 0.05$). (G) Plasma activity of MMP-9 was assessed by gelatin zymography experiments. Plasma activity of MMP-9 was significantly increased in ApoE$^{-/-}$ mice treated with URB597 compared to ApoE$^{-/-}$ treated with vehicle (959 ± 1012 vs. 495 ± 307 IOD, $p < 0.05$).

monocytes, macrophages and T cells. However, we found significantly increased numbers of neutrophil cells as wells as significantly diminished levels of collagen structures in atherosclerotic lesions in mice that were treated with the FAAH inhibitor. This was accompanied by an increased aortic expression as well as an increased plasma activity of the matrix-degrading enzyme matrix metalloproteinase-9.

There are only few studies in the field of cardiovascular medicine investigating the effects of FAAH deficiency in mice. The first study suggested rather beneficial effects of genetic FAAH deficiency in mice. Increased levels of AEA due to genetic disruption of FAAH were associated with reduced age-related cardiac dysfunction, myocardial nitrative stress, inflammatory gene expression, and apoptosis in mice. The authors reported that AEA dose dependently attenuated TNF-α-induced ICAM-1 and VCAM-1 expression, NF-κB activation in HCAECs, and the adhesion of monocytes to HCAECs in a CB1- and CB2-dependent manner [27]. The same group also reported rather detrimental effects of FAAH deficiency, suggesting pleiotropic effects of FAAH deficiency depending on the selected experimental model and type of tissue analyzed. In the latter study, doxorubicin-induced cardiotoxic effects such as oxidative and nitrative stress were enhanced by increased AEA levels in a CB1-dependent manner in mice [28]. However, our in vivo experiments did not reveal any impact of FAAH inhibition on plaque size and vascular monocyte infiltration in ApoE$^{-/-}$ mice, which were fed a proatherogenic diet for eight weeks. Interestingly, we observed reduced collagen structures covering atherosclerotic lesions in ApoE$^{-/-}$ mice that received the selective FAAH inhibitor compared with vehicle. A thin fibrous cap characterizes advanced, unstable atherosclerotic lesion that are prone to rupture. Thus, our experiments suggest that FAAH inhibition is accompanied with rather detrimental effects during atherogenesis.

In this context, a clinical study investigating the levels of endocannabinoids in patients suffering from acute coronary syndrome found that levels of AEA were higher in patients with unstable angina pectoris compared with patients having stable disease conditions [29]. Though, one might assume that this instability induces increased AEA levels, it is conceivable that increased levels of AEA possess a causative role and destabilize atherosclerotic lesions by initiating degradation of vascular collagen fibers. Important enzymes that digest components of extracellular matrix, such as collagen and elastin, are so-called matrix metalloproteinases (MMP)-zinc-dependent endopeptidases, which are expressed by inflammatory cells in atherosclerotic lesions. We found increased aortic expression of matrix metalloproteinase-9 in ApoE$^{-/-}$ mice treated with the selective FAAH inhibitor, thus having increased levels of AEA. In this context, a recent study suggests that AEA induces matrix metalloproteinase-2 production through CB1 and transient receptor potential vanilloid 1 (TRPV1) in human dental pulp cells in culture [30]. Mukhopadhyay et al. also demonstrated that AEA dependent myocardial tissue injury was essentially regulated by CB1 since cardiotoxic effects such as oxidative and nitrative stress were damped under concomitant CB1 inhibition [28]. It seems conceivable that AEA also induces matrix metalloproteinases in a CB1 dependent manner in our experimental model. Taken together, inhibition of FAAH increases the accumulation of neutrophil cells in atherosclerotic lesions and fosters plaque vulnerability by increasing vascular expression as well as plasma activity of matrix metalloproteinase-9 during atherogenesis in mice.

Disclosure statement

The authors confirm that there are no conflicts of interest.

Acknowledgments

This study was supported by Bonfor, and the German Research Foundation DFG (FOR926 project CP1, BMBF project LOGIN). The excellent technical assistance of Kathrin Paul and Heike Slomka is greatly appreciated.

References

[1] Ross R. Atherosclerosis — an inflammatory disease. N Engl J Med 1999;340:115–26.
[2] Hansson GK. Inflammation, atherosclerosis, and coronary artery disease. N Engl J Med 2005;352:1685–95.
[3] Dutta P, Courties G, Wei Y, Leuschner F, Gorbatov R, Robbins CS, et al. Myocardial infarction accelerates atherosclerosis. Nature 2012;487:325–9.
[4] Mach F, Steffens S. The Role of the endocannabinoid system in atherosclerosis. J Neuroendocrinol 2008;20:53–7.
[5] Steffens S, Veillard NR, Arnaud C, Pelli G, Burger F, Staub C, et al. Low dose oral cannabinoid therapy reduces progression of atherosclerosis in mice. Nature 2005;434:782–6.
[6] Xu H, Cheng CL, Chen M, Manivannan A, Cabay L, Pertwee RG, et al. Anti-inflammatory property of the cannabinoid receptor-2-selective agonist JWH-133 in a rodent model of autoimmune uveoretinitis. J Leukoc Biol 2007;82:532–41.
[7] Malfait AM, Gallily R, Sumariwalla PF, Malik AS, Andreakos E, Mechoulam R, et al. The nonpsychoactive cannabis constituent cannabidiol is an oral anti-arthritic therapeutic in murine collagen-induced arthritis. Proc Natl Acad Sci U S A 2000;97:9561–6.
[8] Sanchez AJ, Gonzalez-Perez P, Galve-Roperh I, García-Merino A. R-(+)-[2,3-dihydro-5-methyl-3-(4-morpholinylmethyl)-pyrrolo-[1,2,3-de]-1,4-benzoxazin-6-yl]-1-naphtalenylmethanone (WIN-2) ameliorates experimental autoimmune encephalomyelitis and induces encephalitogenic T cell apoptosis: partial involvement of the CB(2) receptor. Biochem Pharmacol 2006;72:1697–706.
[9] Arevalo-Martin A, Vela JM, Molina-Holgado E, Borrell J, Guaza C. Therapeutic action of cannabinoids in a murine model of multiple sclerosis. J Neurosci 2003;23:2511–6.
[10] Pertwee RG. Pharmacological actions of cannabinoids. Handb Exp Pharmacol 2005;168:1–51.
[11] Schlosburg JE, Kinsey SG, Lichtman AH. Targeting fatty acid amide hydrolase (FAAH) to treat pain and inflammation. AAPS J 2009;11:39–44.
[12] Bátkai S, Pacher P, Osei-Hyiaman D, Radaeva S, Liu J, Harvey-White J, et al. Hypertension endocannabinoids acting at cannabinoid-1 receptors regulate cardiovascular function in hypertension. Circulation 2004;110:1996–2002.
[13] Justinova Z, Mangieri RA, Bortolato M, Chefer SI, Mukhin AG, Clapper JR, et al. Fatty acid amide hydrolase inhibition heightens anandamide signaling without producing reinforcing effects in primates. Biol Psychiatry 2008;64:930–7.
[14] Cravatt BF, Demarest K, Patricelli MP, Bracey MH, Giang DK, Martin BR, et al. Supersensitivity to anandamide and enhanced endogenous cannabinoid signaling in mice lacking fatty acid amide hydrolase. Proc Natl Acad Sci U S A 2001;98:9371–6.
[15] Chang L, Luo L, Palmer JA, Sutton S, Wilson SJ, Barbier AJ, et al. Inhibition of fatty acid amide hydrolase produces analgesia by multiple mechanisms. Br J Pharmacol 2006;148:102–13.
[16] Piomelli D, Tarzia G, Duranti A, Tontini A, Mor M, Compton TR, et al. Pharmacological profile of the selective FAAH inhibitor KDS-4103 (URB597). CNS Drug Rev 2006;12:21–38.
[17] Russo R, Loverme J, La Rana G, Compton TR, Parrott J, Duranti A, et al. The fatty acid amide hydrolase inhibitor URB597 reduces neuropathic pain after oral administration in mice. J Pharmacol Exp Ther 2007;322:236–42.
[18] Montecucco F, Burger F, Mach F, Steffens S. CB2 cannabinoid receptor agonist JWH-015 modulates human monocyte migration through defined intracellular signaling pathways. Am J Physiol Heart Circ Physiol 2008;294:H1145–55.
[19] Zhao Y, Yuan Z, Liu Y, Xue J, Tian Y, Liu W, et al. Activation of cannabinoid CB2 receptor ameliorates atherosclerosis associated with suppression of adhesion molecules. J Cardiovasc Pharmacol 2010;55:292–8.
[20] Hoyer FF, Steinmetz M, Zimmer S, Becker A, Lütjohann D, Buchalla R, et al. Atheroprotection via cannabinoid receptor-2 is mediated by circulating and vascular cells in vivo. J Mol Cell Cardiol 2011;51:1007–14.
[21] Montecucco F, Di Marzo V, da Silva RF, Vuilleumier N, Capettini L, Lenglet S, et al. The activation of the cannabinoid receptor type 2 reduces neutrophilic protease-mediated vulnerability in atherosclerotic plaques. Eur Heart J 2012;33:846–56.
[22] Dol-Gleizes F, Paumelle R, Visentin V, Marés AM, Desitter P, Hennuyer N, et al. Rimonabant a selective cannabinoid CB1 receptor antagonist, inhibits atherosclerosis in LDL receptor-deficient mice. Arterioscler Thromb Vasc Biol 2009;29:12–8.
[23] Tiyerili V, Zimmer S, Jung S, Wassmann K, Naehle CP, Lütjohann D, et al. CB1 receptor inhibition leads to decreased vascular AT1 receptor expression, inhibition of oxidative stress and improved endothelial function. Basic Res Cardiol 2010;105:465–77.
[24] Vilela LR, Medeiros DC, Rezende GH, de Oliveira AC, Moraes MF, Moreira FA. Effects of cannabinoids and endocannabinoid hydrolysis inhibition on pentylenetetrazole-induced seizure and electroencephalographic activity in rats. Epilepsy Res 2013;104:195–202.
[25] Moreira FA, Kaiser N, Monory K, Lutz B. Reduced anxiety-like behaviour induced by genetic and pharmacological inhibition of the endocannabinoid-degrading enzyme fatty acid amide hydrolase (FAAH) is mediated by CB1 receptors. Neuropharmacology 2008;54:141–50.
[26] Murphy N, Cowley TR, Blau CW, Dempsey CN, Noonan J, Gowran A, et al. The fatty acid amide hydrolase inhibitor URB597 exerts anti-inflammatory effects in hippocampus of aged rats and restores an age-related deficit in long-term potentiation. J Neuroinflammation 2012;9:79.

[27] Bátkai S, Rajesh M, Mukhopadhyay P, Haskó G, Liaudet L, Cravatt BF, et al. Decreased age-related cardiac dysfunction, myocardial nitrative stress, inflammatory gene expression, and apoptosis in mice lacking fatty acid amide hydrolase. Am J Physiol Heart Circ Physiol 2007;293:H909–18.
[28] Mukhopadhyay P, Horváth B, Rajesh M, Matsumoto S, Saito K, Bátkai S, et al. Fatty acid amide hydrolase is a key regulator of endocannabinoid induced myocardial tissue injury. Free Radic Biol Med 2011;50:179–95.
[29] Sugamura K, Sugiyama S, Nozaki T, Matsuzawa Y, Izumiya Y, Miyata K, et al. Activated endocannabinoid system in coronary artery disease and antiinflammatory effects of cannabinoid 1 receptor blockade on macrophages. Circulation 2009;119:28–36.
[30] Miyashita K, Oyama T, Sakuta T, Tokuda M, Torii M. Anandamide induces matrix metalloproteinase-2 production through cannabinoid-1 receptor and transient receptor potential vanilloid-1 in human dental pulp cells in culture. J Endod 2012;38:786–90.